



Kinetic fractionation of carbon and oxygen isotopes during hydration of carbon dioxide

Richard E. Zeebe*

School of Ocean and Earth Science and Technology, Department of Oceanography, University of Hawaii at Manoa, 1000 Pope Road, MSB 629, Honolulu, HI 96822, USA

Received 19 November 2013; accepted in revised form 3 May 2014; available online 21 May 2014

Abstract

Kinetic isotope effects (KIEs) during the inorganic hydration of carbon dioxide (CO_2) in aqueous solution cause reduced stable carbon and oxygen isotope ratios ($^{13}\text{C}/^{12}\text{C}$ and $^{18}\text{O}/^{16}\text{O}$) in the reaction product carbonic acid (H_2CO_3) or bicarbonate ion (HCO_3^-), relative to CO_2 . While such KIEs are of importance in various physicochemical, geochemical, and biological systems, very few experimental and theoretical studies have attempted to determine the magnitude of the carbon and oxygen kinetic isotope fractionation (KIF) during hydration of CO_2 . Here I use transition state theory (TST) and quantum chemistry calculations to investigate the reaction rates of isotopic reactants $\text{CO}_2 + n\text{H}_2\text{O}$ ($n = 1-8$) along the hydration pathway to H_2CO_3 or HCO_3^- . Locating transition states is difficult and the quantum chemistry calculations time-consuming at large n . My results suggest that the hydration mechanism for $n = 1-3$ is unlikely to be the dominant pathway producing KIFs during CO_2 hydration in aqueous solution; hydration mechanisms for $n \geq 4$ appear more likely. For $n = 4-8$, the predicted KIF based on MP2/aug-cc-pVDZ calculations at 25 °C is $\sim 1.023-1.033$ and $\sim 1.013-1.015$, for carbon and oxygen, respectively. However, these values are uncertain and the results of the present study suggest that new experimental work is required to accurately determine the KIF of carbon and oxygen during CO_2 hydration.

© 2014 Elsevier Ltd. All rights reserved.

1. INTRODUCTION

The hydration of carbon dioxide in aqueous solution plays a central role in numerous physicochemical, geochemical, and biological systems (for review, see Kern, 1960). Understanding the molecular mechanism and determining/predicting the rate of the hydration reaction both theoretically and experimentally continues to be a highly active research area (Nguyen et al., 1997, 2008; Stirling and Pápai, 2010; Wang et al., 2010; Wang and Cao, 2013). In addition, kinetic isotope effects (KIEs) during the hydration of CO_2 and dehydration of HCO_3^- provide insight into various geochemical processes, including formation of cryogenic carbonates, non-equilibrium isotope effects in speleothem

calcite, diffusion-reaction coupling in boundary layers, air–sea gas exchange, mineral precipitation in surface and deep-sea corals, and more (e.g. Clark and Lauriol, 1992; Mickler et al., 2004; Zeebe and Wolf-Gladrow, 2001; Guo, 2008; McConnaughey, 1989; Adkins et al., 2003; Uchikawa and Zeebe, 2012).

Despite its geochemical significance, very few experimental studies have attempted to determine the kinetic isotope fractionation (KIF) during hydration/dehydration of $\text{CO}_2/\text{HCO}_3^-$ (Marlier and O’Leary, 1984; Clark and Lauriol, 1992; Guo, 2008). Moreover, the available data is inconsistent (see Section 5.2). To the best of my knowledge, there has been no theoretical study so far on KIF during CO_2 hydration and only one theoretical study on KIF during HCO_3^- dehydration (Guo, 2008). The present study provides insight into the hydration mechanism and estimates the kinetic fractionation of carbon and oxygen isotopes during CO_2 hydration based on transition state

* Tel.: +1 (808) 956 6473; fax: +1 (808) 956 7112.
E-mail address: zeebe@soest.hawaii.edu

theory (Section 2) and quantum chemistry calculations (Section 3). The theoretical results obtained here (Section 4) and results from earlier experimental studies will be discussed in Section 5.

2. THEORY

2.1. Isotope effect in transition state theory

For the reader unfamiliar with the application of transition state theory (TST) to isotope effects, a brief summary is given here. The rate constant of a chemical reaction based on TST may be written as (Eyring, 1935):

$$k = \frac{k_B T}{h} \kappa K_{\ddagger}, \quad (1)$$

where k_B and h is Boltzmann's and Planck's constant, respectively, T is temperature (in Kelvin), κ is a transmission coefficient, and K_{\ddagger} is the equilibrium constant between the activated state molecules in the transition state (index \ddagger) and the reactants (A, B, \dots). The equilibrium constant can be determined from statistical mechanics:

$$K_{\ddagger} = \frac{Q_{\ddagger}}{Q_A Q_B \dots}, \quad (2)$$

where Q_i 's are partition functions (Urey, 1947; Bigeleisen and Mayer, 1947). While absolute values of rate constants for chemical reactions may be difficult to predict accurately based on TST, rate constant ratios for isotopic molecules are often more reliable:

$$\frac{k}{k'} = \frac{\kappa}{\kappa'} \frac{K_{\ddagger}}{K'_{\ddagger}} = \frac{\kappa}{\kappa'} \frac{Q_{\ddagger}}{Q'_{\ddagger}} \frac{Q'_A Q'_B \dots}{Q_A Q_B \dots}, \quad (3)$$

where primes denote quantities of the isotopically heavier molecule (hence $k/k' > 1$ for normal isotope effects). Application of statistical mechanics then leads to the following expression for the rate constant ratio (for review, see Bigeleisen and Wolfsberg, 1958; Kubicki, 2008; Wolfsberg et al., 2010):

$$\begin{aligned} \frac{k}{k'} &= \frac{\kappa}{\kappa'} \frac{\omega_L^{\ddagger}}{\omega_L'^{\ddagger}} \times R_{\sigma} \times R_A \times R_B \times \dots \times (R_T)^{-1} \\ &= \frac{\kappa}{\kappa'} \frac{\omega_L^{\ddagger}}{\omega_L'^{\ddagger}} \times R_{\sigma} \times R_u \times R_{\text{exc}} \times R_{\text{zpe}} \end{aligned} \quad (4)$$

where R_A, R_B, \dots, R_T are partition function ratios (PFRs) of reactant molecules (A, B, \dots) and TS (missing one vibrational mode), ω_L^{\ddagger} is the TS's imaginary frequency of decomposition (see below), and:

$$R_{\sigma} = \frac{\sigma}{\sigma'} \times \dots \times \left(\frac{\sigma^{\ddagger}}{\sigma'^{\ddagger}} \right)^{-1} \quad (5)$$

$$R_u = \prod_i^{3n-6} \frac{u'_i}{u_i} \times \dots \times \left(\prod_i^{3n-7} \frac{u'_i}{u_i} \right)^{-1} \quad (6)$$

$$R_{\text{exc}} = \prod_i^{3n-6} \frac{1 - e^{-u_i}}{1 - e^{-u'_i}} \times \dots \times \left(\prod_i^{3n-7} \frac{1 - e^{-u_i}}{1 - e^{-u'_i}} \right)^{-1} \quad (7)$$

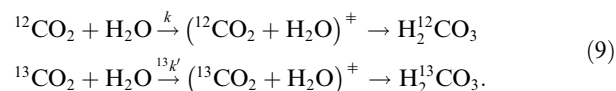
$$R_{\text{zpe}} = \prod_i^{3n-6} \frac{e^{-u_i/2}}{e^{-u'_i/2}} \times \dots \times \left(\prod_i^{3n-7} \frac{e^{-u_i/2}}{e^{-u'_i/2}} \right)^{-1}, \quad (8)$$

where σ 's are symmetry numbers, $u_i = hc\omega_i/k_B T$, and ω_i 's are the fundamental vibrational frequencies of the molecules. Ellipsis indicate that the first term on the right is to be repeated for all reactant molecules. For linear molecules, the sums run from 1 to $3n - 5$ and $3n - 6$ for reactants and TS, respectively. Note that the TS is missing one vibrational degree of freedom. This decomposition mode corresponds to translation along the reaction coordinate, also referred to as a nongenuine vibration with imaginary frequency ω_L^{\ddagger} .

The transmission coefficient κ takes into account the classical effect that a system with sufficient energy to surmount the energy barrier may still be reflected; κ also takes into account the quantum mechanical effect of tunneling, which allows a system to tunnel through the energy barrier even though it has insufficient energy in a classical sense. Significant effects from tunneling should be expected for light elements such as hydrogen but much less so for carbon and oxygen e.g. (Melander and Saunders, 1980; Felipe et al., 2003). Thus the assumption $\kappa/\kappa' = 1$ is made here. However, effects from reflection and tunneling on the rate constants cannot be excluded and it needs to be kept in mind that such effects are not included in the calculations presented here (see Section 5). Given the fundamental vibrational frequencies of the reactant molecules and TS (ω_i 's) obtained from quantum chemistry calculations (see below), rate constant ratios k/k' were calculated using Eq. (4) and Eqs. (5)–(8) with $\kappa/\kappa' = 1$.

2.2. Carbon isotope ratios and rate constants

In order to evaluate the predictions for the KIF during CO_2 hydration as obtained here, one must be able to compare theoretical and experimental results. For example, consider the formation of a small amount of H_2CO_3 from a large pool of CO_2 in aqueous solution ($\text{O} = {}^{16}\text{O}$, if not stated otherwise):



It is easy to show that the reaction constants and carbon isotope ratios of H_2CO_3 (instantaneous, no reverse reaction) and CO_2 are related by:

$$\frac{{}^{13}k'}{k} = \frac{{}^{13}R_{\text{H}_2\text{CO}_3}}{{}^{13}R_{\text{CO}_2}} \quad (10)$$

where ${}^{13}k'$ and k is the rate constant for dissolved ${}^{13}\text{C}^{16}\text{O}^{16}\text{O}$ and ${}^{12}\text{C}^{16}\text{O}^{16}\text{O}$, respectively. The concentrations of these two isotopologues will be denoted by $[3]_d$ and $[2]_d$ for short (notation follows Gao and Marcus, 2001). Furthermore, $[\text{H}_2{}^{13}\text{C}^{16}\text{O}^{16}\text{O}] = [3]_z$ and $[\text{H}_2{}^{12}\text{C}^{16}\text{O}^{16}\text{O}] = [2]_z$. Then the rate expressions for reactions (9) read:

$$\begin{aligned} d[2]_z/dt &= [2]_z = k [2]_d \\ d[3]_z/dt &= [3]_z = {}^{13}k' [3]_d. \end{aligned} \quad (11)$$

For the formation of a small amount of H_2CO_3 from a large reactant CO_2 pool, we may assume the ${}^{12}\text{CO}_2$ and ${}^{13}\text{CO}_2$ concentrations to be constant. Hence $[2]_z = k [2]_d \times t$ and $[3]_z = {}^{13}k' [3]_d \times t$. Using the definition of carbon isotope ratios in H_2CO_3 and CO_2 , we can write:

$$\frac{{}^{13}R_{\text{H}_2\text{CO}_3}}{{}^{13}R_{\text{CO}_2}} = \frac{[3]_z/[2]_z}{[3]_d/[2]_d} = \frac{{}^{13}k'[3]_d/k[2]_d}{{}^{13}k'} \quad (12)$$

Thus, the ${}^{13}\text{C}/{}^{12}\text{C}$ rate constant ratio for the hydration of CO_2 is simply equal to the carbon isotope ratio of instantaneously formed H_2CO_3 divided by the carbon isotope ratio of the CO_2 reactant pool. While the result for carbon isotopes seems intuitively obvious, for oxygen isotopes it is not (see below). If the carbon isotope ratios of H_2CO_3 and CO_2 can be determined analytically, theory and experiment can be directly compared. Note that in practice, ${}^{13}R_{\text{H}_2\text{CO}_3}$ may be determined indirectly after quantitative conversion of H_2CO_3 to HCO_3^- and/or CO_3^{2-} (all kinetically produced carbonate must be extracted from solution to capture the KIE).

2.3. Oxygen isotope ratios and rate constants

The relationship between isotope ratios and rate constants is more complex for oxygen than for carbon. First, multiply substituted isotopologues in CO_2 and H_2CO_3 are possible for oxygen. Second, different oxygen isotopes can substitute in non-equivalent positions in the molecules (Fig. 1), leading to isotopomers with different properties (Guo, 2008). Third, the mass of the oxygen coming from the water during hydration needs to be considered.

In the following, the different oxygen positions in the reacting CO_2 and H_2O molecules and at the transition state will be denoted by a, b, and c (for illustration of $n = 1$, see Fig. 1). The positions may be characterized as follows: (a) passive (O on CO_2 , not involved in H-transfer at TS), (b) active (O on CO_2 , involved in H-transfer at TS), (c) water oxygen (O_w), forming new C– O_w bond. Simply based on these positions, the largest KIF can already be expected for C and O_w , as these positions are associated with the largest bond changes and hence changes in partition function ratios between reactants and TS (see Section 2.1).

The hydration reaction involving n water molecules may be written as:

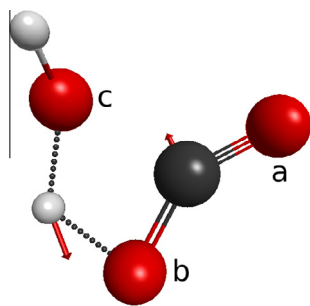
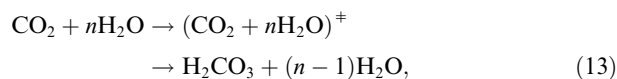
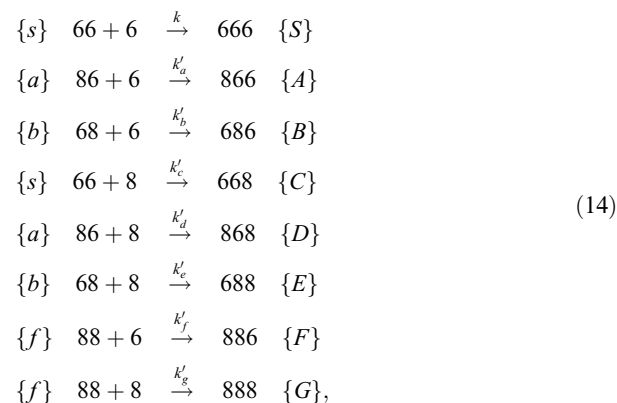


Fig. 1. Transition state geometry for $\text{CO}_2 + n\text{H}_2\text{O}$ at $n = 1$ (TS-1) based on MP2/aug-cc-pVDZ level of theory. Black = carbon, red = oxygen, white = hydrogen. Arrows indicate the normal mode of decomposition, corresponding to translation along the reaction coordinate. Labels a, b, and c indicate different oxygen positions in the reacting molecules (see text). (For interpretation of the references to color in this figure legend, the reader is referred to the web version of this article.)



where $\text{CO}_2 + n\text{H}_2\text{O}$ refers to a pre-reaction complex (Nguyen et al., 1997, 2008; Wang and Cao, 2013). For $n > 1$, the pre-complex geometry is generally non-symmetric with regard to oxygen exchange on CO_2 . Thus, in general, positions a and b not only differ in the TS structure but also in the CO_2 pre-complex (see Fig. 6). Considering the different positions and all ${}^{16}\text{O}$ and ${}^{18}\text{O}$ combinations leads to the following reactions:



where symbols in braces on the left and right are abbreviations for the concentrations of isotopologues/isotopomers of CO_2 and H_2CO_3 , respectively. For instance, $a = [86] = \text{C}^{18}\text{O}^{16}\text{O}$, $A = [866] = \text{H}_2\text{C}^{18}\text{O}^{16}\text{O}^{16}\text{O}$, etc. (notation after Gao and Marcus, 2001; Uchikawa and Zeebe, 2012). Note that the concentrations of molecules $a = [86]$ and $b = [68]$, for instance, correspond to the positions a and b as described above (Fig. 1). Furthermore, $[6] = [\text{H}_2^{16}\text{O}]$, $[8] = [\text{H}_2^{18}\text{O}]$, and $R_w = [8]/[6]$.

In analogy to carbon isotopes, I define an overall KIF for oxygen (${}^{18}\text{O}/{}^{16}\text{O}$):

$$\frac{{}^{18}k'}{k} := \frac{{}^{18}R_{\text{H}_2\text{CO}_3}}{{}^{18}R_{\text{CO}_2}}, \quad (15)$$

where ${}^{18}R_{\text{H}_2\text{CO}_3}$ is the instantaneous oxygen isotope ratio of H_2CO_3 formed from CO_2 and H_2O without back-reaction. If the ${}^{18}\text{R}$'s of these compounds can be determined analytically relative to a standard, the oxygen KIF can be measured (in practice, ${}^{18}R_{\text{H}_2\text{CO}_3}$ may have to be determined indirectly). Reactant CO_2 and H_2O are assumed to be in equilibrium with respect to oxygen isotopes. Note that ${}^{18}k'$ represents an overall rate constant but is not associated with a single, elementary reaction. The oxygen isotope ratios are given by (in e.g. H_2CO_3 count total $[{}^{18}\text{O}] = U$ vs. total $[{}^{16}\text{O}] = V$):

$${}^{18}R_{\text{H}_2\text{CO}_3} = \frac{A + B + C + 2(D + E + F) + 3G}{3S + 2(A + B + C) + D + E + F} = \frac{U}{V} \quad (16)$$

$${}^{18}R_{\text{CO}_2} = \frac{a + b + 2f}{2s + a + b} = \frac{X}{Y} = \frac{x}{y}, \quad (17)$$

where U , V , X , and Y are total oxygen concentrations and x and y are total oxygen abundances.

Fortunately, only a subset of the isotopologues/isotopomers (cf. Eq. (14)) need to be considered to determine the oxygen isotope ratios of H_2CO_3 and CO_2 . For instance, if

the oxygen isotopes in CO₂ were stochastically distributed, then:

$${}^{18}R_{\text{CO}_2} = \frac{xy + yx + 2x^2}{2y^2 + xy + yx} = \frac{2xy + 2x^2}{2y^2 + 2xy} = \frac{x}{y}. \quad (18)$$

To derive this result, consider the probability for two consecutive draws of oxygen atoms from a pool. For a stochastic distribution, the overall ¹⁸O/¹⁶O ratio would also be simply given by:

$${}^{18}R_{\text{CO}_2} = \frac{2xy}{2y^2} = \frac{x}{y} = \left(\frac{a+b}{2s}\right)_{\text{stoch.}}, \quad (19)$$

which would only require considering reactions involving *a*, *b*, and *s*. However, the distribution of ¹⁸O/¹⁶O in the CO₂ pre-complex is not exactly stochastic, one reason being that *a* ≠ *b* because the two positions are energetically non-equivalent. Such differences may be evaluated by assuming ¹⁸O fractionations in *a*, *b*, and *f* relative to the stochastic distribution:

$$\begin{aligned} a' &= \alpha_a xy \\ b' &= \alpha_b yx \\ f' &= \alpha_f x^2, \end{aligned} \quad (20)$$

where primes denote abundances of CO₂ molecules. Writing Eq. (17) in terms of abundances and inserting yields (*s'* = *y*²):

$$\begin{aligned} {}^{18}R_{\text{CO}_2} &= \frac{xy(\alpha_a + \alpha_b) + 2\alpha_f x^2}{2y^2 + xy(\alpha_a + \alpha_b)} = \frac{\alpha xy + \alpha_f x^2}{y^2 + \alpha xy} \\ &= \frac{\alpha x}{y} \cdot \frac{y + \alpha_f \alpha^{-1} x}{y + \alpha x} = \frac{\alpha x}{y} \cdot \Gamma, \end{aligned} \quad (21)$$

where $\alpha = (\alpha_a + \alpha_b)/2$. Because $x \ll y$, Γ is very close to 1. Calculated partition function ratios for *a*/*s*, *b*/*s*, and *f*/*s* relative to water typically differ by less than 2‰ (see *K_a* and *K_b* below), indicating that the distribution of ¹⁸O/¹⁶O in the CO₂ pre-complex is very close to the stochastic distribution. Even if α_a , α_b , and α_f were in the order of ±10‰, Γ would differ from 1 by only 0.06‰. Hence, the following is a very good approximation for the current purpose:

$$\begin{aligned} {}^{18}R_{\text{CO}_2} &\simeq \frac{\alpha x}{y} = \frac{(\alpha_a + \alpha_b)x}{2y} = \frac{a'/y + b'/y}{2y} = \frac{a' + b'}{2y^2} \\ &= \frac{a + b}{2s}. \end{aligned} \quad (22)$$

Similar arguments yield:

$${}^{18}R_{\text{H}_2\text{CO}_3} \simeq \frac{A + B + C}{3S}. \quad (23)$$

As a result, only paired reactions involving *a*, *b*, and *s* (for CO₂) and *A*, *B*, *C*, and *S* (for H₂CO₃) will be considered in the following. The rate expressions for these reactions read:

$$\begin{aligned} \dot{S} &= [666] = k [66][6] = k s [6] \\ \dot{A} &= [866] = k'_a [86][6] = k'_a a [6] \\ \dot{B} &= [686] = k'_b [68][6] = k'_b b [6] \\ \dot{C} &= [668] = k'_c [66][8] = k'_c s [8]. \end{aligned} \quad (24)$$

Assuming again a large, equilibrated reactant pool, *s*, *a*, *b*, [6], and [8] can be taken as constant. As a result, \dot{S} , \dot{A} , \dot{B} , and \dot{C} are constant, leading to $S = k s [6] \times t$, etc. It follows that $A/S = \dot{A}/\dot{S} = (k'_a/k)(a/s)$, $B/S = \dot{B}/\dot{S} = (k'_b/k)(b/s)$, and $C/S = \dot{C}/\dot{S} = (k'_c/k)([8]/[6])$. Note that the last rate expression in Eq. (24) for \dot{C} involves [8], rather than [6]. It may also be written as $\dot{C} = k'_c s [6] R_w$. Thus, compared to the other rate expressions, it also involves the isotope ratio of the water.

One more step is necessary to calculate isotope ratios from reactants and rate constant ratios (Eqs. (22) and (23)) because concentrations such as *a*, *b*, etc. and isotope ratios *a*/*s*, *b*/*s*, etc. can not easily be evaluated. However, ratios such as (*a*/*s*)/*R_w* may be evaluated using partition function ratios determined from quantum chemistry calculations (see below). Hence, write ¹⁸R_{CO₂}, for example, as:

$${}^{18}R_{\text{CO}_2} = \frac{[a/s + b/s]/R_w}{2/R_w}. \quad (25)$$

Recall that *a*, *b*, and *s* are equilibrium reactant concentrations and consider the following equilibria for substitutions in the pre-complex (in which generally [86] ≠ [68]):

$$66 + 8 \rightleftharpoons 86 + 6; \quad K_a = \frac{[86][6]}{[66][8]} = \frac{Q_a/Q_s}{Q_8/Q_6} = \frac{a/s}{R_w} \quad (26)$$

$$66 + 8 \rightleftharpoons 68 + 6; \quad K_b = \frac{[68][6]}{[66][8]} = \frac{Q_b/Q_s}{Q_8/Q_6} = \frac{b/s}{R_w}, \quad (27)$$

where *Q*'s are partition functions. Thus, we have:

$${}^{18}R_{\text{CO}_2} = \frac{K_a + K_b}{2/R_w}. \quad (28)$$

Note that the oxygen isotope ratio of water, *R_w*, ultimately drops out of the calculation (see below). The ratio ¹⁸R_{H₂CO₃} is evaluated similarly, but in this case by dividing numerator and denominator by (*S* × *R_w*) instead of (*s* × *R_w*) and using the rate expressions (Eq. (24)) to eliminate *A*/*S*, *B*/*S*, and *C*/*S*. The individual terms are:

$$\begin{aligned} \frac{A/S}{R_w} &= \frac{k'_a}{k} \frac{a/s}{R_w} \frac{[6]}{[6]} = \frac{k'_a}{k} K_a \\ \frac{B/S}{R_w} &= \frac{k'_b}{k} \frac{b/s}{R_w} \frac{[6]}{[6]} = \frac{k'_b}{k} K_b \\ \frac{C/S}{R_w} &= \frac{k'_c}{k} \frac{s/s}{R_w} \frac{[8]}{[6]} = \frac{k'_c}{k}, \end{aligned} \quad (29)$$

yielding:

$${}^{18}R_{\text{H}_2\text{CO}_3} = \frac{\frac{k'_a}{k} K_a + \frac{k'_b}{k} K_b + \frac{k'_c}{k}}{3/R_w} \quad (30)$$

and thus finally:

$$\frac{{}^{18}R'}{k} = \frac{{}^{18}R_{\text{H}_2\text{CO}_3}}{R_w} = \frac{2}{3} \cdot \frac{\frac{k'_a}{k} K_a + \frac{k'_b}{k} K_b + \frac{k'_c}{k}}{K_a + K_b}. \quad (31)$$

For convenience, one may define $K := (K_a + K_b)/2$ (see Table 4). Note that for all pre-complexes tested here, *K_a* and *K_b* were nearly identical (difference <2‰). If *K_a* = *K_b* = *K*, the expression above can be simplified to:

$$\frac{{}^{18}R'}{k} = \frac{1}{3} \left(\frac{k'_a}{k} + \frac{k'_b}{k} + \frac{k'_c}{k} K^{-1} \right), \quad (32)$$

which is just the average of the individual rate constant ratios, except for the third term. The factor K^{-1} arises because the oxygen KIF is defined relative to CO_2 , rather than H_2O (Eq. (15)). In this definition, the fractionation for positions a and b between the TS and CO_2 depends on the KIF associated with k'_a/k and k'_b/k but is independent of the bulk isotope composition of CO_2 . However, the isotope ratio associated with position c of the TS (relative to CO_2) depends on k'_c/k , as well as the bulk isotope composition of the water (see text following Eq. (24)). Because oxygen isotope equilibrium was assumed between reactant CO_2 and H_2O (see above), the calculation yields the factor K^{-1} , representing the pre-complex CO_2 -water equilibrium (Eqs. (26) and (27)). Note also that if there were no differences in rate constants ($k'_i = k$), Eq. (31) simplifies to:

$$^{18}\alpha_{av} := 2/3 + 2/3(K_a + K_b)^{-1}, \quad (33)$$

which represents the average oxygen isotope ratio of reactants ($\text{CO}_2 + \text{H}_2\text{O}$) relative to that of CO_2 (see below).

2.4. Summary of carbon and oxygen isotope fractionation

The relationship between equilibrium and kinetic fractionation of carbon and oxygen isotopes for CO_2 hydration/ HCO_3^- dehydration in water is illustrated in Fig. 2. Note that in the following the KIF for (i) $\text{CO}_2 + \text{H}_2\text{O} \rightarrow \text{H}_2\text{CO}_3$ and (ii) $\text{CO}_2 + \text{H}_2\text{O} \rightarrow \text{H}^+ + \text{HCO}_3^-$ will be treated synonymously for two reasons. First, it turns out that the hydration step in water may proceed via (ii), rather than (i) (see below). Second, if the KIF is determined analytically by quantitative conversion of dissolved carbonate to HCO_3^- and/or CO_3^{2-} (all kinetically produced carbonate is extracted from solution), then the KIFs associated with pathways (i) and (ii) cannot be distinguished from one another. However, it needs to be kept in mind that in reality there is an offset between the isotopic compositions of H_2CO_3 and HCO_3^- , with equilibrium values being established quasi-instantaneously (e.g. Eigen et al., 1961; Zeebe and Wolf-Gladrow, 2001).

The present calculations provide an estimate for the carbon KIF during CO_2 hydration, $^{13}k'/k$ (Fig. 2 and Eq. (10)). The difference in the carbon KIF for the hydration of dissolved CO_2 and the dehydration of HCO_3^- is equal to the equilibrium fractionation factor between HCO_3^- and CO_2 (Fig. 2), which has a value of $\sim 9\text{‰}$ at 25 °C (Zhang et al., 1995) (only approximate values are used in the illustration to simplify the discussion). Thus, the present results may be compared to experimentally determined values for the carbon KIF either during CO_2 hydration or HCO_3^- dehydration – in case of the latter, the equilibrium fractionation needs to be taken into account.

The present calculations also provide an estimate for the oxygen KIF during CO_2 hydration, $^{18}k'/k$ (Fig. 2 and Eq. (31)). Without fractionation/subsequent oxygen exchange, the isotope ratio of HCO_3^- unidirectionally produced from CO_2 and H_2O is simply given by the average of the reactant ratios:

$$^{18}R_{\text{HCO}_3^-} = 2/3^{18}R_{\text{CO}_2} + 1/3^{18}R_{\text{H}_2\text{O}}. \quad (34)$$

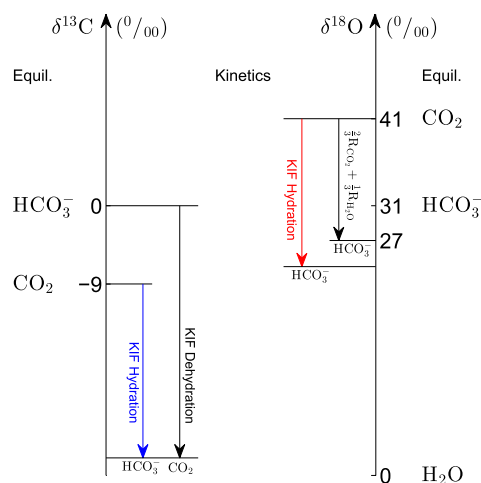


Fig. 2. Schematic illustration of equilibrium and kinetic isotope fractionation (KIF) of carbon and oxygen during CO_2 hydration and HCO_3^- dehydration in water. Numbers to the left and right of the $\delta^{13}\text{C}$ and $\delta^{18}\text{O}$ axis, respectively, indicate approximate equilibrium δ -values. Kinetic isotope effects are illustrated in the center. The $\delta^{13}\text{C}$ of HCO_3^- and the $\delta^{18}\text{O}$ of water are arbitrarily set to zero. Both reaction products HCO_3^- and dissolved CO_2 unidirectionally produced by hydration of CO_2 and dehydration of HCO_3^- are depleted in carbon isotopes relative to the reactants (left axis). The difference in carbon KIF is equal to the equilibrium fractionation between HCO_3^- and CO_2 of $\sim 9\text{‰}$ at 25 °C (Zhang et al., 1995). The oxygen isotope composition of HCO_3^- unidirectionally produced from dissolved CO_2 and H_2O without fractionation is $\sim 27\text{‰}$ at 25 °C, the average of the reactant compositions (right axis). Deviations from that value indicate isotope effects due to different rate constants for different isotopologues/isotopomers (see text). Arrows in blue and red labeled 'KIF hydration' are the KIFs theoretically determined here (Eqs. (10) and (31)). (For interpretation of the references to color in this figure legend, the reader is referred to the web version of this article.)

Assuming CO_2 - H_2O equilibrium and dividing by $^{18}R_{\text{CO}_2}$ gives:

$$\frac{^{18}R_{\text{HCO}_3^-}}{^{18}R_{\text{CO}_2}} = 2/3 + 1/3K_{eq}^{-1}, \quad (35)$$

where $K_{eq} = ^{18}\alpha_{(\text{CO}_2-\text{H}_2\text{O}(l))}$. Eq. (35) is identical to Eq. (31) for $K_{eq} = K$ and $k'_i/k = 1$, cf. Eq. (33). In other words, the overall oxygen KIF expressed here as an isotope ratio (Eq. (31)) is just the average of the reactant isotope ratios in case the rate constants were all the same ($k'_i = k$). Thus, the deviation from this average value measures the oxygen KIE during CO_2 hydration due to differences in isotopic rate constants for different isotopologues/isotopomers. For example, dissolved CO_2 equilibrated with water at $\delta^{18}\text{O}_{\text{H}_2\text{O}} = 0\text{‰}$ has a $\delta^{18}\text{O}$ -value of $\sim 41\text{‰}$ (Beck et al., 2005) and hence the $\delta^{18}\text{O}$ of the unidirectionally produced HCO_3^- would be $\sim 27\text{‰}$ (average reactant value, see Fig. 2). Thus, a deviation in the measured HCO_3^- value from 27‰ would indicate the effect of the rate constants on the oxygen KIE during CO_2 hydration.

3. QUANTUM CHEMISTRY CALCULATIONS

The rate constant ratios required to determine the carbon and oxygen KIF during CO₂ hydration were obtained using quantum chemistry calculations. Locating equilibrium structures, which represent minima on the potential energy surface (PES) is relatively easy. Locating TS structures is much more difficult as these geometries represent saddle points on the PES (e.g. Jensen, 1995). Although initial trial structures for the CO₂ + *n*H₂O TS were adopted from the literature (Nguyen et al., 1997, 2008; Wang and Cao, 2013), locating TSs indeed turned out to be challenging and the quantum chemistry calculations time-consuming at large *n*. Even when mode following was turned on and runs were initiated very close to a TS (located at a different level of theory), TS geometry searches often drifted towards a different TS or did not converge at all after several hundred iterations.

Note that directly using previous TS geometries and frequencies (Nguyen et al., 2008; Wang and Cao, 2013) to determine KIFs for all *n* = 1–8 was not an option here. KIFs at different *n* need to be determined at the *same* level of theory to allow for a meaningful comparison. However, several geometries adopted from Nguyen et al. (2008) (*n* = 1–4) and Wang and Cao (2013) (*n* = 5, 6, 8) had been obtained at *different* levels of theory by both groups. Note also that while e.g. Nguyen et al. (2008) used a higher level of theory (MP2/aug-cc-pVTZ vs. MP2/aug-cc-pVDZ used here), it ultimately turned out that different TS geometries at higher *n* seem to have a much larger effect on calculated KIFs than a more complete basis set (see below).

Searches for equilibrium (pre-complex) and TS geometries were performed using the quantum-chemistry package GAMESS (Gordon and Schmidt, 2005) in parallel execution on a 88-CPU Linux cluster. For the structures studied here, all geometry optimizations were followed by Hessian runs to check whether the normal mode analysis yielded indeed exactly zero and one imaginary frequency (ω) for equilibrium and TS geometries, respectively. Different basis sets and levels of theory were tested, including B3LYP/6-311+G(2df,2p) and MP2/aug-cc-pVDZ (B3G and MP2Z in the following), similar to those used in recent quantum chemistry studies of CO₂ hydration (Nguyen et al., 2008; Wang and Cao, 2013). B3G gave somewhat higher values than MP2Z, for instance, for the KIF of carbon at 25 °C (by ~1.5‰ and ~3‰ at *n* = 3 and *n* = 6, respectively). However, B3G strongly underestimated the ¹³C equilibrium fractionation between HCO₃⁻ and CO₂(g) at *n* = 7, while MP2Z yielded too low values for the ¹⁸O equilibrium fractionation between CO₂/HCO₃⁻ and H₂O (see Section 4.1). For several equilibrium/TS geometries, stationary points located at MP2Z (zero/one imaginary ω) did not correspond to stationary points at B3G (one/two or more imaginary ω). Obviously, neither of the two methods is perfect. However, results at different *n* can only be compared when internally consistent, i.e. when obtained with the same method (in the following MP2Z, unless stated otherwise).

Pre-complex structures, intermediate states, and final reaction products were obtained using IRC (intrinsic reaction coordinate) runs starting at the previously located TS. IRC runs were usually performed at the HF/aug-cc-pVDZ

level, except for TS-8b (full MP2/aug-cc-pVDZ level, see below). All stationary geometries obtained during IRC runs were re-optimized at the full MP2/aug-cc-pVDZ level before the structures were employed for frequency and isotope calculations. Continuum solvation methods were also tested, including the Polarizable Continuum Model (PCM) for water. However, switching PCM on (all else being equal) occasionally produced additional imaginary ω 's, i.e. indicating non-equilibrium or non-stationary points on the PES as affected by the solvation model. At this stage it is not clear whether this behavior is due to inadequacies in the solvation method or whether such structures are actually non-stationary in real aqueous solutions. The results reported below were obtained without solvation models.

4. RESULTS

4.1. Test: Equilibrium fractionation factors

A first-order test for the quantum chemistry methods employed here is to check calculated carbon and oxygen equilibrium fractionation factors against values that are known from experimental studies. Equilibrium fractionation factors for several compounds relevant for the present study have been measured quite accurately, including ¹³ $\alpha_{(\text{HCO}_3^- - \text{CO}_2(\text{g}))}$, ¹⁸ $\alpha_{(\text{CO}_2(\text{g}) - \text{H}_2\text{O}(\text{l}))}$, and ¹⁸ $\alpha_{(\text{HCO}_3^- - \text{H}_2\text{O}(\text{l}))}$. Theoretical equilibrium fractionation factors were calculated here as described in Zeebe (2009, 2010). Both MP2Z and B3G yield fundamental frequencies in close agreement with experimental values for all molecules (Fig. 3). One exception is the frequency of the bicarbonate CO–H stretching mode ($\omega_{\text{CO-H}}$), which is typically overestimated in quantum chemistry calculations relative to the observed value in solution (Rudolph et al., 2006, 2008; Guo, 2008). However, this has no effect on the calculated carbon isotope fractionation because $\omega_{\text{CO-H}}$ (~3000 cm⁻¹) falls in a much higher frequency band than the HCO₃⁻-modes that are sensitive to carbon mass (~600–1600 cm⁻¹). Omission of the CO–H stretch from the calculations yielded no change in the predicted ¹³ $\alpha_{(\text{HCO}_3^- - \text{CO}_2(\text{g}))}$. The same holds true for the calculated kinetic fractionation of stable carbon isotopes.

However, the CO–H stretching mode does affect oxygen isotope fractionation. For example, ¹⁸ $\alpha_{(\text{HCO}_3^- - \text{H}_2\text{O}(\text{l}))}$ increases with $\omega_{\text{CO-H}}$, when keeping the frequency ratio $\omega_{\text{CO-H}}/\omega'_{\text{CO-H}}$ constant. Thus, because the quantum chemistry calculations tend to overestimate $\omega_{\text{CO-H}}$, one might expect ¹⁸ $\alpha_{(\text{HCO}_3^- - \text{H}_2\text{O}(\text{l}))}$ to be overestimated as well, provided that the theoretical frequency ratio is accurate. However, the opposite is the case (Table 1), suggesting that the overestimated CO–H stretch does not lead to excessively large values for the calculated oxygen isotope fractionation. On the other hand, potential errors in the calculated ratio $\omega_{\text{CO-H}}/\omega'_{\text{CO-H}}$ cannot be excluded. In summary, while the overpredicted CO–H stretching mode has no effect on the calculated carbon isotope fractionation, it is a potential source of error in the calculated oxygen isotope fractionation. This applies to both the HCO₃⁻ equilibrium fractionation, as well as kinetic effects associated with the CO–H stretch in the CO₂ + *n*H₂O transition state.

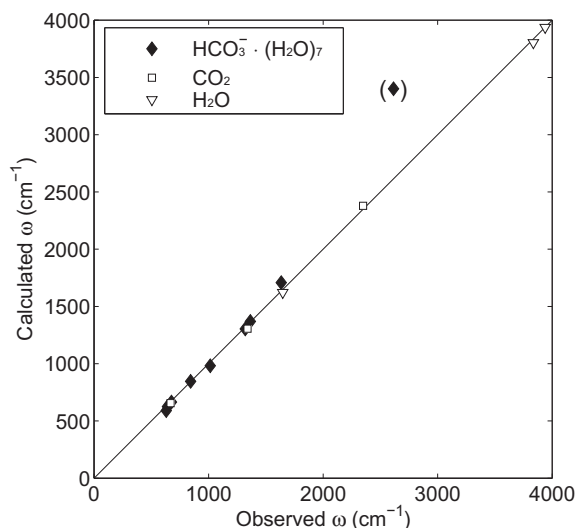


Fig. 3. Calculated vs. observed frequencies of molecules relevant to CO_2 hydration. Theoretical ω 's were obtained at MP2/aug-cc-pVDZ; all frequencies unscaled. The bicarbonate CO–H stretching mode is shown in parentheses.

Table 1

Comparison between calculated^a and experimental equilibrium fractionation factors at 25 °C.

Method ^b	$^{13}\alpha_{(\text{HCO}_3^- - \text{CO}_2(\text{g}))}$	$^{18}\alpha_{(\text{CO}_2(\text{g}) - \text{H}_2\text{O}(\text{l}))}$	$^{18}\alpha_{(\text{HCO}_3^- - \text{H}_2\text{O}(\text{l}))}$
MP2Z	1.0069	1.0358 ^c	1.0277 ^c
B3G	1.0045	1.0415 ^c	1.0290 ^c
Exp.	1.0079 ^d	1.0412 ^e	1.0311 ^f

^a All frequencies unscaled. α 's involving HCO_3^- based on $\text{HCO}_3^- \cdot (\text{H}_2\text{O})_7$ -cluster.

^b MP2Z = MP2/aug-cc-pVDZ, B3G = B3LYP/6-311+G(2df,2p).

^c Using $^{18}\alpha_{(\text{H}_2\text{O}(\text{l}) - \text{H}_2\text{O}(\text{g}))} = 1.0094$ (Majoube, 1971).

^d Zhang et al. (1995).

^e O'Neil et al. (1975).

^f Uchikawa and Zeebe (2013).

Excluding the bicarbonate CO–H stretch, the calculated frequency scaling factors for both MP2Z and B3G were close to 1.0 for the combined frequencies of CO_2 , H_2O and $\text{HCO}_3^- \cdot (\text{H}_2\text{O})_7$ (Fig. 3). Hence unscaled frequencies were used in the present study. Note that the HCO_3^- frequencies and fractionation factors involving HCO_3^- were calculated based on a $\text{HCO}_3^- \cdot (\text{H}_2\text{O})_7$ -cluster. This cluster corresponds to the reaction product of $\text{CO}_2 + n\text{H}_2\text{O}$ (except for one proton) at $n = 8$, the largest n considered here to determine kinetic isotope fractionations. Considering an even larger hydration shell ($n \geq 10$) is important for accurately calculating equilibrium oxygen isotope fractionation between dissolved carbonate species and water (Zeebe, 2009). However, in the present context it is more important to evaluate the quantum chemistry results at smaller n , corresponding to the number of water molecules and cluster sizes used to determine the KIF. Moreover, it turned out that the calculated KIF for oxygen was rather insensitive to n (see below).

The results obtained with MP2Z show good agreement with the observed ^{13}C equilibrium fractionation between HCO_3^- and $\text{CO}_2(\text{g})$ at 25 °C based on the $\text{HCO}_3^- \cdot (\text{H}_2\text{O})_7$ -cluster (Table 1). B3G underestimates this value by more than 40%. However, this result is sensitive to conformation and often shows better agreement for larger clusters (Rustad et al., 2008; Hill et al., 2014). On the other hand, MP2Z yields too low values for the ^{18}O equilibrium fractionation between CO_2 and H_2O , while B3G shows good agreement. Based on calculations for the $\text{HCO}_3^- \cdot (\text{H}_2\text{O})_7$ -cluster, MP2Z and B3G both underestimate $^{18}\alpha_{(\text{HCO}_3^- - \text{H}_2\text{O}(\text{l}))}$ (by $\sim 2\%$ and 3% , respectively), possibly due to a small number of hydrating water molecules included in the simulations (e.g. Zeebe, 2009; Hill et al., 2014). The bottom line is that while a few results for the calculated equilibrium fractionation factors indicate poor performance of the quantum chemistry methods, others are encouraging. Note, however, that even a good performance in terms of equilibrium fractionation is no guarantee for accurate predictions of KIFs due to additional uncertainties, including the predicted transition state geometry and transition state theory itself (Section 2.1). Unless stated otherwise, calculated results for KIFs will be reported for MP2Z below for consistency reasons (see Section 3), with the caveat that the results may have uncertainties similar to or larger than those for equilibrium fractionation factors.

4.2. $\text{CO}_2 + n\text{H}_2\text{O}$ transition state geometries

4.2.1. $n = 1, 2, 3$

The transition from $\text{CO}_2 + n\text{H}_2\text{O}$ to H_2CO_3 encompasses three major changes in molecular structure, which may be illustrated for $n = 1$ (in the following, oxygen indices will indicate positions, see Fig. 1). (I) Formation of the new $\text{C}-\text{O}_c$ bond, (II) breaking of the water O_c-H bond, and (III) formation of the new O_b-H bond. For $n = 1$, the proton involved in II and III is the same. All three changes occur simultaneously and there is only one TS along the reaction path. For $n = 2$ and 3, the proton transfer occurs via a proton relay along the chain of two and three water molecules, respectively (Fig. 4). Nevertheless, all changes still occur essentially simultaneously, and for the structures probed here, there is only one TS along the reaction path for $n \leq 3$ (concerted pathway).

4.2.2. $n = 4, 5, 6, 8$

For $n \geq 4$, the reaction proceeds stepwise through a $\text{HCO}_3^- - \text{H}_3\text{O}^+$ intermediate state and a second TS appears (TS- $n-2$), separating processes I + II (TS- $n-1$) from the proton relay and the formation of the new O_b-H bond (Figs. 4 and 5). Note that a direct reaction pathway $\text{CO}_2 + \text{H}_2\text{O} \rightarrow \text{HCO}_3^-$ and a stepwise hydration mechanism have been discussed earlier (Eigen et al., 1961, 1964; Stirling and Pápai, 2010). The stepwise hydration mechanism was also identified in quantum chemistry calculations for $n \geq 5$ (Wang and Cao, 2013) and was found here for $n = 4$ as well. The total MP2Z energies (E_i) of TS-4-2 and TS-4-1 are nearly identical and $\sim 22 \text{ kcal mol}^{-1}$ higher than E_i of the pre-complex R-4 (Table 2 and Fig. 5). However, the calculated carbon KIF for TS-4-2 is close to zero and $\sim 22\%$ lower than

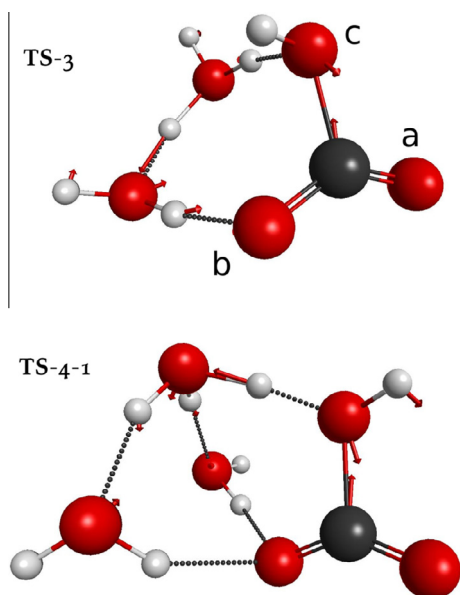


Fig. 4. Transition state geometries at $n = 3$ (TS-3) and $n = 4$ (TS-4-1) based on MP2/aug-cc-pVDZ level of theory. Arrows indicate the normal mode of decomposition. Note proton relay and H-transfer to O_b in TS-3, which is absent in TS-4-1.

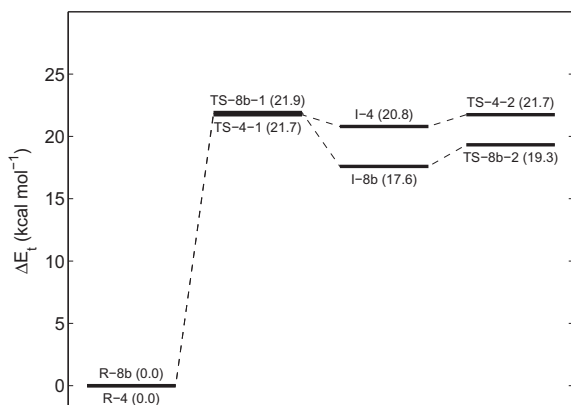


Fig. 5. Differences in total MP2 energies of transition states (TS) and intermediate states (I) at $n = 4$ and $n = 8$ (b) relative to the respective pre-complex energies of reactants (R).

for TS-4-1 (see below). TS-4-2 is associated with the proton relay, whereas the formation of the C– O_c bond is already complete, i.e. the carbon atom is already part of the HCO_3^- -structure. Thus, TS-4-2 is not relevant for determining the carbon KIF during CO_2 hydration. Rather, the carbon KIF is governed by the rate limiting step for the C– O_c bond formation, i.e. the step from R-4 to TS-4-1.

All TSs for $n \geq 4$ for which KIFs were determined below (corresponding to TS- $n-1$ or simply TS- n) show the separation of the proton relay from processes I + II. For $n = 8$, two different TS geometries were tested (Fig. 6). In TS-8a, the $\text{CO}_2 + \text{H}_2\text{O}$ reaction center is peripherally hydrogen-bonded to a cage-like structure of seven water molecules, which subsequently facilitate the proton relay. In TS-8b,

Table 2
Properties of selected geometries: transition state (TS), reactant pre-complex (R), and intermediate state (I).

	$d(\text{C}-\text{O}_c)$ (Å)	ω_L^\ddagger (cm^{-1})	Energy (a.u.) ^a
TS-1	1.7011	1707.04i	−264.351897
TS-2	1.6082	1101.34i	−340.653409
TS-3	1.5665	841.70i	−416.921037
R-4	3.1487	–	−493.257519
TS-4-1	1.5986	534.16i	−493.222882
I-4	1.4836	–	−493.224384
TS-4-2	1.4467	519.93i	−493.222870
TS-5	1.6210	601.00i	−569.503460
TS-6	1.6292	597.35i	−645.780878
TS-8a	1.6333	586.72i	−798.339978
R-8b	3.3438	–	−798.375285
TS-8b-1	1.8253	176.85i	−798.340359
I-8b	1.4093	–	−798.347251
TS-8b-2	1.3776	924.01i	−798.344488

^a Total MP2 energy (MP2/aug-cc-pVDZ).

the reaction center is hydrogen-bonded to a cluster of five-water molecules on one, and two on the opposite side, where the five-water cluster is involved in the proton transfer. The different geometries lead to different properties of the TS. For instance, the distance along the forming C– O_c bond is ~ 0.2 Å longer in TS-8b than in TS-8a (Table 2). Also, formation of the C– O_c bond (I) and breaking of the water O_c –H bond (II) occur essentially simultaneously in TS-8a. In contrast, IRC runs at the full MP2Z level revealed that in TS-8b, process II only occurs after process I is nearly complete (i.e. after the C– O_c distance has dropped from 1.83 to 1.48 Å).

The calculated difference in total energies (ΔE_t) for both TS-4-1 and TS-8b-1 relative to the respective pre-complex energies is ~ 22 kcal mol^{−1} (Fig. 5). An experimental value for the Gibbs energy of activation (ΔG^\ddagger) for CO_2 hydration in water at 25 °C was recently given as 21.8 kcal mol^{−1} (Wang et al., 2010). However, the agreement of the numbers is coincidental as ΔE_t and ΔG^\ddagger are different quantities. The experimental value for ΔG^\ddagger is based on the Eyring relationship between rate constant and $\Delta G^\ddagger = \Delta H^\ddagger - T\Delta S^\ddagger$, where ΔH^\ddagger and ΔS^\ddagger are the enthalpy and entropy of activation, respectively. Estimation of ΔG^\ddagger from quantum chemistry calculations requires additional steps that include consideration of level of theory, correlation methods, zero-point energies, solvation models, basis set-specific frequency scaling factors, etc. The details have been discussed elsewhere and values of ~ 19 kcal mol^{−1} ($n = 4$, in water) and 17–26 kcal mol^{−1} ($n = 8$, in water) in agreement with observations have been reported (Nguyen et al., 2008; Wang and Cao, 2013).

4.3. $^{13}\text{C}/^{12}\text{C}$ kinetic isotope fractionation

Based on the transition state geometries described above, the KIF for stable carbon isotopes ($^{13}k'/k$) during CO_2 hydration was calculated for $n = 1$ –8 using the equations given in Sections 2.1 and 2.2. For both carbon and oxygen, the results will be reported as the inverse ratio

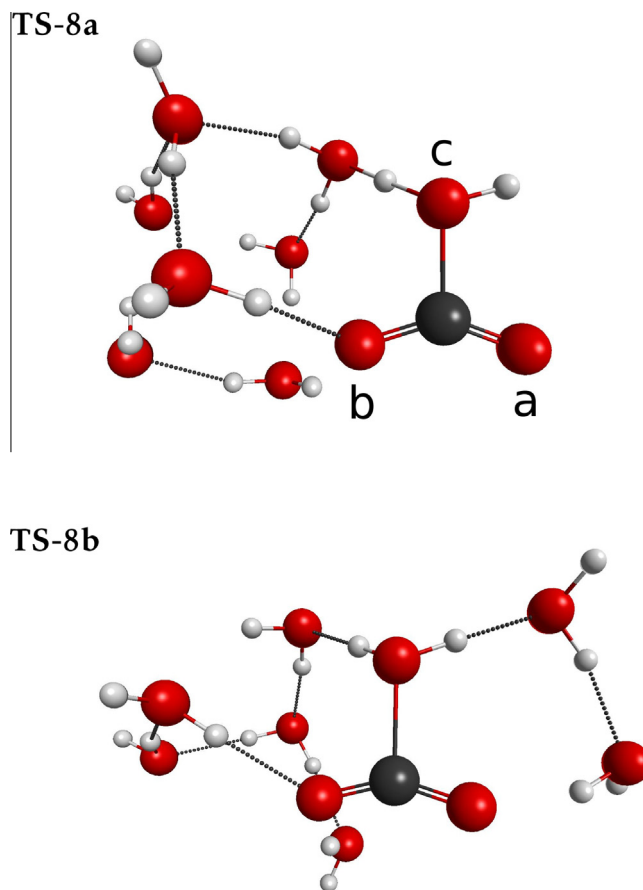


Fig. 6. Transition state geometries at $n = 8$ (TS-8a and TS-8b) based on MP2/aug-cc-pVDZ level of theory. Note elongated C–O_c and reduced H–O_c distances in TS-8b relative to TS-8a.

k^M/k' ($M = 13, 18$) to obtain simple numbers > 1 for normal isotope effects. When expressed as a δ -value, $^M\delta(k/k')$ refers to:

$$^M\delta(k/k') = (k^M/k' - 1) \times 1000. \quad (36)$$

The calculated kinetic isotope fractionation for carbon increases slightly from 10‰ to 14‰ as n increases from 1 to 3, jumps suddenly by about +9‰ between $n = 3$ and $n = 4$, and remains fairly constant for $n = 4$ –6 (Table 3 and Fig. 8). The jump corresponds to the switch from a one-step hydration mechanism to a multi-step hydration mechanism at $n \geq 4$ as described above. The largest contribution to the jump ($\sim 6.5\%$) is due to the change in the ratio of the decomposition mode, $\omega_L^\ddagger/\omega_L'^\ddagger$ (Table 3). In TS-3, the entire water chain facilitating the proton relay is involved in the nongenuine vibration along the decomposition path (Fig. 4). However, in TS-4-1, the decomposition mode almost exclusively involves the C–O_c–H group that participates in the formation of the new C–O_c bond and the breaking of the water O_c–H bond (Fig. 4), lowering $|\omega_L^\ddagger|$ by $\sim 300 \text{ cm}^{-1}$ (Table 3). As a result, the decomposition mode for $n = 4$ is more sensitive to carbon mass than for $n = 3$, which explains the increase in $\omega_L^\ddagger/\omega_L'^\ddagger$. Note that the jump in the carbon KIF is solely due to changes in the TS and not in the pre-complex as there is virtually no change in the

Table 3
Results for carbon KIF at 25 °C.^a

n	R_A^b	R_T	$\omega_L^\ddagger/\omega_L'^\ddagger$	$k/^{13}k'$
1	1.1918 ^c	1.1846	1.0039	1.0101
2	1.1916	1.1829	1.0058	1.0133
3	1.1915	1.1788	1.0033	1.0141
4 (1)	1.1914	1.1758	1.0098	1.0232
4 (2)	1.1914	1.1910	1.0010	1.0014
5	1.1916	1.1772	1.0103	1.0226
6	1.1918	1.1771	1.0108	1.0234
8 (a)	1.1913	1.1770	1.0110	1.0233
8 (b)	1.1913	1.1703	1.0144	1.0326

^a All results obtained at MP2/aug-cc-pVDZ; all frequencies unscaled.

^b β -factor of CO₂ · n H₂O pre-complex.

^c Non-stationary (one imaginary ω).

β -factor (R_A) of the CO₂ · n H₂O pre-complex between $n = 3$ and $n = 4$ (Table 3). The remainder of the jump ($\sim 2.5\%$) is due to a general decline in R_T as n increases (recall that $k/k' \propto R_A/R_T$, see Eq. (4)). The carbon bonding in the TS progressively weakens and R_T drops with increasing n , relative to the pre-complex (Table 3).

For $n = 8$, the two different TS geometries (TS-8a and TS-8b, see Fig. 6) lead to significantly different values for the calculated KIF of carbon, with $k/^{13}k'$ being about 9‰ larger for TS-8b (Table 3 and Fig. 8). The carbon atom is less strongly bound in TS-8b (closer resembling a CO_2^- than a HCO_3^- -structure), hence giving a smaller R_T and a larger carbon KIE. In addition, ω_L^\ddagger is substantially lower and the C–O_c distance larger in TS-8b (Table 2). The decomposition mode in TS-8b largely consists of a displacement of the bend CO_2 skeleton against the mostly rigid water unit. In contrast, the decomposition mode in TS-8a also involves breaking of the water O_c–H bond. This makes ω_L^\ddagger more sensitive to carbon mass in TS-8b relative to TS-8a. As a result, the calculated $\omega_L^\ddagger/\omega_L^{\ddagger'}$ ratio and hence the predicted carbon KIF is larger for TS-8b.

For most TS geometries tested here, the predicted temperature dependence of the carbon KIF for CO_2 hydration is relatively weak over the temperature range $T_C = 0$ – 100 °C, except for TS-8b (Fig. 7). Over this range, the temperature slope is about +0.5, –2.0, and –5.7‰/100 °C, for $n = 2$, 8(a), and 8(b), respectively. The contribution of the decomposition mode ($\omega_L^\ddagger/\omega_L^{\ddagger'}$) to the KIF is independent of temperature. Hence the temperature dependence is determined by the ratio R_A/R_T (Eq. (4)). Because of similarities in several genuine vibrations of the pre-complex and TS, R_A and R_T also show a similar temperature dependence, particularly for small n . For example, at $n = 2$, R_A and R_T both drop in nearly identical fashion by ~7% between 0 and 100 °C. Over this range, R_T drops slightly quicker than R_A , leading to a small increase in $k/^{13}k'$ with temperature at $n = 2$. However, for $T_C > 120$ °C, the opposite is true, leading to a decrease in $k/^{13}k'$, which finally approaches the high-temperature limit $\omega_L^\ddagger/\omega_L^{\ddagger'}$ (Fig. 7).

4.4. $^{18}\text{O}/^{16}\text{O}$ kinetic isotope fractionation

As expected, the smallest oxygen KIF is predicted for position a (passive, see Section 2.3), with k/k'_a varying between ~2‰ and 5‰ for $n = 2$ –8 (Table 4). The predicted KIF is larger for position b (active), with values for k/k'_b of

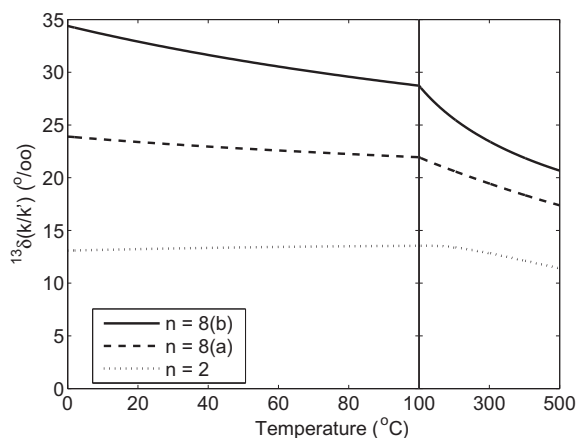


Fig. 7. Calculated temperature dependence of kinetic carbon isotope fractionation for the CO_2 hydration reaction $\text{CO}_2 + n\text{H}_2\text{O}$ at different n based on MP2/aug-cc-pVDZ.

up to ~11‰. Except for TS-8b, an inverse KIE is predicted when considering only k/k'_c , which measures the KIF in position c relative to $^{16}\text{O}/^{18}\text{O}$ in water (Section 2.3). In other words, oxygen in position c is calculated to be more strongly bound in the TS than in H_2O , which is plausible given the (albeit loose) C–O bond in the TS vs. the O–H bond in water. Predicted values for k/k'_c range roughly between –16‰ and 0‰ (the latter applies to TS-8b with largely unaltered H–O_c–H water molecule). However, because the oxygen KIF is defined relative to CO_2 (rather than H_2O), the relevant quantity for position c is $K \cdot k/k'_c$ (see Section 2.3), which varies between ~27‰ and 37‰. Finally, because the overall oxygen KIF is basically an average of the KIF for the three positions (Eq. (32)), $k/^{18}k'$ varies between ~10‰ and 15‰ for $n = 1$ –8 (Table 4 and Fig. 8). The values of $k/^{18}k'$ and $^{18}\alpha_{av}^{-1}$ (Eq. (33)) differ only slightly, indicating a small contribution of different isotopologue-/isotopomer rate constants to the total oxygen KIF.

5. DISCUSSION

The present study predicts a substantially larger carbon KIF during CO_2 hydration for $n \geq 4$ compared to $n < 4$ (Fig. 8). While absolute values calculated here carry considerable uncertainties (see below), the predicted carbon-to-oxygen ratio of the KIF is probably more robust. For $n < 4$, the calculated ratio is similar, while for $n \geq 4$, the carbon KIF is larger than the oxygen KIF by a factor of ~1.5 to 2.2 (TS-8b). The stepwise hydration mechanism is responsible for the larger carbon KIF for $n \geq 4$. The mechanism involves a larger number of water molecules participating in the proton relay and hence appears more likely to be the dominant pathway in aqueous solution. Thus, I suggest that during CO_2 hydration in aqueous solution, the carbon KIF should be significantly larger than the oxygen KIF, which can be tested experimentally.

5.1. Theoretical and computational uncertainties

As mentioned above, transition state theory as applied here is subject to uncertainties, including unknown effects from transmission and tunneling (although tunneling effects should be much smaller for carbon and oxygen than e.g. hydrogen, see Melander and Saunders, 1980). In addition, the present calculation of partition functions is based on the harmonic approximation, ignoring possible effects of anharmonicity in the molecular vibrations. Computational limitations include uncertainties in the predicted TS geometries due to imperfect basis sets, correlation methods, and solvent effects. In order to simulate solvent effects in aqueous solution more realistically, $n > 8$ may be desirable, particularly for oxygen isotope fractionation (e.g. Zeebe, 2009). Unfortunately, computations with large n turned out to be cumbersome and computationally expensive for the current system. Alternatively, solvation models may be applied, which have their own limitations, however (see Section 3).

As a result, one important limitation of the present study is the small number of different TSs at a given n that

Table 4
Results for oxygen KIF at 25 °C.^a

n	k/k'_a	k/k'_b	k/k'_c	$K \cdot k/k'_c$ ^b	$^{18}\alpha_{av}^{-1}$	$k/^{18}k'$
1 ^c	0.9985	1.0052	0.9925	1.0361	1.0142	1.0130
2	1.0022	1.0028	0.9844	1.0270	1.0140	1.0105
3	1.0024	1.0106	0.9938	1.0333	1.0129	1.0153
4	1.0042	1.0082	0.9934	1.0337	1.0132	1.0152
5	1.0032	1.0067	0.9917	1.0289	1.0122	1.0128
6	1.0038	1.0067	0.9905	1.0286	1.0125	1.0129
8 (a)	1.0046	1.0062	0.9937	1.0310	1.0122	1.0138
8 (b)	1.0037	1.0048	1.0000	1.0371	1.0121	1.0150

^a All results obtained at MP2/aug-cc-pVDZ; all frequencies unscaled.

^b $K = (K_a + K_b)/2$, see text.

^c Pre-complex non-stationary (one imaginary ω).

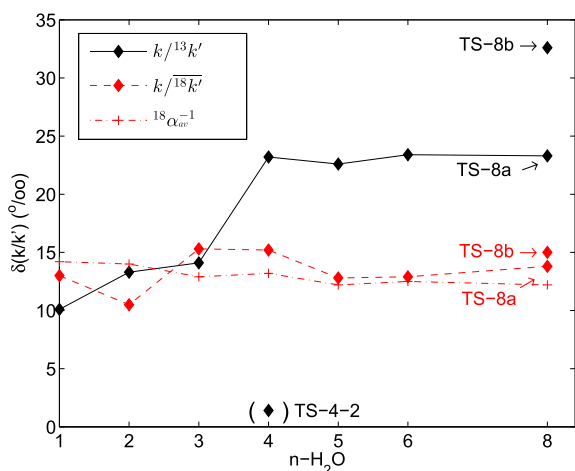


Fig. 8. Calculated carbon and oxygen kinetic isotope fractionation for the CO_2 hydration reaction $\text{CO}_2 + n\text{H}_2\text{O}$ at different n based on MP2/aug-cc-pVDZ.

could be sampled to determine KIFs, particularly at larger n (Fig. 8). Because the number of possible TSs usually grows quickly with n , ideally one might like to combine quantum chemistry and molecular dynamics approaches to sample as many TSs as possible. However, to obtain accurate energy barriers, frequencies, etc., a high level of theory is required, which makes this approach very expensive. Future theoretical studies of the present system should also improve the treatment of tunneling and recrossing, which may require tools such as variational transition state theory (e.g. Truhlar and Garrett, 1984).

Despite the theoretical and computational uncertainties, there are at least three aspects of the calculated results that lend confidence in the methods applied. First, the predicted molecular frequencies of relevant equilibrium structures are in excellent agreement with observations, except for the bicarbonate CO–H stretching mode (Fig. 3). Second, the calculated equilibrium fractionation factors based on MP2Z are in reasonable to good agreement with experimental values, more so for carbon than for oxygen (Section 4.1). Third, while the two items above are relevant for testing equilibrium geometries, the agreement between observed and predicted energy barriers for the CO_2

hydration in water (see Section 4.2.2) suggest that quantum chemistry calculations at sufficiently high level of theory are also capable of accurately predicting $\text{CO}_2 + n\text{H}_2\text{O}$ transition state geometries (Nguyen et al., 2008; Wang et al., 2010; Wang and Cao, 2013). The overall magnitude of uncertainties associated with the calculated KIFs is estimated to be similar to or larger than those for equilibrium fractionation factors (see Section 4.1).

5.2. Experimental studies

Marlier and O'Leary (1984) reported a carbon KIF for CO_2 hydration in water of 6.9‰ at 24 °C (Table 5). However, the study was subsequently cited by the same group with a value of 13.0‰ (O'Leary et al., 1992). Clark and Lauriol (1992) reported a carbon KIF for HCO_3^- dehydration in water of 32.0‰ at 0 °C. Taking into account a ~12‰ equilibrium fractionation at 0 °C between HCO_3^- and dissolved CO_2 (Zhang et al., 1995), yields a KIF for the hydration reaction of 19.7‰ (Table 5). The discrepancy between O'Leary et al. (1992) and Clark and Lauriol (1992) of about 7‰ in $k/^{13}k'$ appears much larger than might be explained by differences in experimental temperatures of 25 K. For comparison, the strongest dependence of $k/^{13}k'$ on temperature was calculated here for TS-8b (Fig. 7), declining by only 1.8‰ between 0 and 25 °C. Thus, the

Table 5
Results from experimental studies for carbon and oxygen KIF during CO_2 hydration (k^+ s) and HCO_3^- dehydration (k_- 's).

$k/^{13}k'$	$^{13}\alpha_{(\text{HCO}_3^- - \text{CO}_2)}$	$k_-/^{13}k'_-$ ^a	Temp. (°C)	$k_-/^{18}k'_-$ ^a
(1.0069) ^b	1.0077 ^b	(1.0147) ^b	24	
1.0130 ^c	1.0090 ^c	1.0220 ^c	25?	
1.0197 ^d	1.0121 ^e	1.0320 ^f	0	
			0	1.0060 ^{-1?f}

^a HCO_3^- dehydration.

^b Marlier and O'Leary (1984). Subsequently cited by same group with different value, see ^c.

^c O'Leary et al. (1992).

^d Calculated.

^e Zhang et al. (1995).

^f Clark and Lauriol (1992), see text.

the currently available experimental data for $k/^{13}k'$ appear to be inconsistent. Guo (2008) performed similar experiments as Clark and Lauriol (1992) but did not report a value for the carbon KIF during HCO_3^- dehydration based on the data.

The results obtained here for the carbon KIF at $n \geq 4$ (Fig. 8) are more compatible with the larger value based on Clark and Lauriol (1992). One of the experimental challenges is to prevent re-equilibration (i.e. hinder the reverse reaction), otherwise the KIE will not be fully expressed. Experimentally determined KIFs then represent minimum values, which may tend to fall below theoretical values. This could be the case here for the predicted carbon KIF at $n \geq 4$, which is larger than the experimental values. However, drawing firm conclusions appears difficult at this stage, given computational uncertainties and inconsistencies between experimental studies. Nevertheless, note that Guo (2008) calculated a value of $\sim 30\%$ for the carbon KIF during HCO_3^- dehydration at $n = 2$ and 25°C based on B3LYP/cc-pVTZ(-f), which is also more consistent with the larger dehydration value given by Clark and Lauriol (1992).

In addition, Clark and Lauriol (1992) reported a value for the oxygen KIF during HCO_3^- dehydration of $\sim 6\%$ at 0°C . While the notation of $^{18}\text{O}/^{16}\text{O}$ rate constant ratios is inconsistent in that paper, the data in Fig. 3 and Table 3 of Clark and Lauriol (1992) shows that CO_2 was enriched in ^{18}O by $\sim 6\%$ relative to CaCO_3 and hence HCO_3^- by inference. In contrast, for the dehydration reaction, Guo (2008) calculated that CO_2 would be depleted in ^{18}O by $\sim 7\%$ relative to HCO_3^- . The bottom line is that oxygen isotope data on the KIF during hydration/dehydration of $\text{CO}_2/\text{HCO}_3^-$ seem even more sparse and inconsistent than for carbon. This author is not aware of a systematic experimental study on the oxygen KIF during CO_2 hydration.

McConnaughey (1989) reported ^{13}C and ^{18}O depletions in rapidly precipitated carbonates from film solutions. However, the solution pH was not controlled in those experiments and varied widely (7.4–8.5) and hence the relative contributions of hydration and hydroxylation to the observed isotope fractionation are unknown. Also, for the experimental setup, equilibrium isotope fractionation factors were not determined (rather estimated) and the data obtained does not allow a mass-balance calculation to track the partitioning of, say, carbon isotopes among gas, liquid, and solid phase. Relative to the calculated calcite-solution equilibrium, the reported ^{13}C and ^{18}O depletions in the precipitated CaCO_3 at 1, 4, and 21°C were $\sim 4\text{--}5\%$ and $\sim 16\%$, respectively (McConnaughey, 1989). These numbers may reflect KIFs during CO_2 hydration/hydroxylation. However, this is uncertain due to a lack of control over mass fluxes and pH in the experiments. It remains unclear whether the precipitation was truly quantitative, whether the reaction time for precipitation allowed for re-equilibration between HCO_3^- and CO_2 , and whether the values (if accurate) would apply to hydration or hydroxylation, or a combination of both. In summary, the currently available data on KIF during CO_2 hydration/ HCO_3^- dehydration is unsatisfactory and hampers a conclusive comparison between theory and experiment.

6. CONCLUSIONS

The present study provides estimates for the kinetic fractionation of carbon and oxygen isotopes during CO_2 hydration ($\text{CO}_2 + n\text{H}_2\text{O}$) based on transition state theory and quantum chemistry calculations. The results indicate that a concerted hydration mechanism ($n = 1\text{--}3$) is unlikely to be the dominant pathway producing KIFs during CO_2 hydration in aqueous solution; a stepwise hydration mechanism ($n \geq 4$) appears more likely. For $n = 4\text{--}8$, the predicted KIF based on MP2/aug-cc-pVDZ calculations at 25°C is $\sim 1.023\text{--}1.033$ and $\sim 1.013\text{--}1.015$, for carbon and oxygen, respectively. However, these values should be taken with caution, given theoretical and computational uncertainties (cf. Section 5.1). Experimental data on kinetic isotope effects during CO_2 hydration/ HCO_3^- dehydration are sparse and inconsistent. New and systematic experimental work is needed to fully understand the hydration/dehydration mechanism in aqueous solution and to accurately determine the magnitude of the associated kinetic isotope effects.

ACKNOWLEDGMENTS

I thank the editor and three anonymous reviewers for their constructive comments. I am grateful to Joji Uchikawa for patiently listening to my BALLOON project ideas. This is Hess-EMatrix contribution #1-0326-42.

APPENDIX A. SUPPLEMENTARY DATA

Supplementary data associated with this article can be found, in the online version, at <http://dx.doi.org/10.1016/j.gca.2014.05.005>.

REFERENCES

- Adkins J. F., Boyle E. A., Curry W. B. and Lutringer A. (2003) Stable isotopes in deep-sea corals and a new mechanism for 'vital effects'. *Geochim. Cosmochim. Acta* **67**, 1129–1143.
- Beck W. C., Grossmann E. L. and Morse J. W. (2005) Experimental studies of oxygen isotope fractionation in the carbonic acid system at $15^\circ, 25^\circ$, and 40°C . *Geochim. Cosmochim. Acta* **69**(14), 3493–3503.
- Bigeleisen J. and Mayer M. G. (1947) Calculation of equilibrium constants for isotopic exchange reactions. *J. Chem. Phys.* **15**, 261–267.
- Bigeleisen J. and Wolfsberg M. (1958) Theoretical and experimental aspects of isotope effects in chemical kinetics. *Adv. Chem. Phys.* **1**, 15–76.
- Clark I. D. and Lauriol B. (1992) Kinetic enrichment of stable isotopes in cryogenic calcites. *Chem. Geol.* **102**(1-4), 217–228.
- Eigen M., Kustin K. and Maass G. (1961) Die Geschwindigkeit der Hydratation von SO_2 in wariger Losung. *Z. Phys. Chem. NF* **30**, 30–136.
- Eigen M., Kruse W., Maass G. and De Maeyer L. (1964) Rate constants of protolytic reactions in aqueous solution. In *Progress in Reaction Kinetics II* (ed. G. Porter). Pergamon, Oxford, pp. 287–318.
- Eyring H. (1935) The activated complex and the absolute rate of chemical reactions. *Chem. Rev.* **17**(1), 65–77.

- Felipe M. A., Kubicki J. D. and Rye D. M. (2003) Hydrogen isotope exchange kinetics between H_2O and H_4SiO_4 from ab initio calculations. *Geochim. Cosmochim. Acta* **67**(7), 1259–1276.
- Gao Y. Q. and Marcus R. A. (2001) Strange and unconventional isotope effects in ozone formation. *Science* **293**, 259–263.
- Gordon M. S. and Schmidt M. W. (2005) Advances in electronic structure theory: GAMESS a decade later. In *Theory and Applications of Computational Chemistry: The First Forty Years* (eds. G. Frenking, K. S. Kim and G. E. Scuseria). Elsevier, Amsterdam, pp. 1167–1189.
- Guo W. (2008) Carbonate clumped isotope thermometry: application to carbonaceous chondrites and effects of kinetic isotope fractionation. Ph. D. thesis, California Institute of Technology.
- Hill P. S., Tripati A. K. and Schauble E. A. (2014) Theoretical constraints on the effects of pH, salinity, and temperature on clumped isotope signatures of dissolved inorganic carbon species and precipitating carbonate minerals. *Geochim. Cosmochim. Acta* **125**, 610–652.
- Jensen F. (1995) Locating transition structures by mode following: a comparison of six methods on the Ar_8 Lennard-Jones potential. *J. Chem. Phys.* **102**, 6,706–6,718.
- Kern D. M. (1960) The hydration of carbon dioxide. *J. Chem. Educ.* **37**, 14–23.
- Kubicki J. D. (2008) Transition state theory and molecular orbital calculations applied to rates and reaction mechanisms in geochemical kinetics. In *Kinetics of Water–Rock Interaction* (eds. S. L. Brantley, J. D. Kubicki and A. F. White). Springer, pp. 39–72.
- Majoube M. (1971) Fractionnement en oxygène 18 et en deutérium entre l'eau et sa vapeur. *J. Chim. Phys.* **68**, 1423–1436.
- Marlier J. F. and O'Leary M. H. (1984) Carbon kinetic isotope effects on the hydration of carbon dioxide and the dehydration of bicarbonate ion. *J. Am. Chem. Soc.* **106**(18), 5054–5057.
- McConnaughey T. (1989) ^{13}C and ^{18}O isotopic disequilibrium in biological carbonates: II. In vitro simulation of kinetic isotope effects. *Geochim. Cosmochim. Acta* **53**, 163–171.
- Melander L. and Saunders W. H. (1980) *Reaction Rates of Isotopic Molecules*. Wiley & Sons, New York, p. 331.
- Mickler P. J., Banner J. L., Stern L., Asmerom Y., Edwards R. L. and Ito E. (2004) Stable isotope variations in modern tropical speleothems: evaluating equilibrium vs. kinetic isotope effects. *Geochim. Cosmochim. Acta* **68**, 4381–4393.
- Nguyen M. T., Matus M. H., Jackson V. E., Ngan V. T., Rustad J. R. and Dixon D. A. (2008) Mechanism of the hydration of carbon dioxide: direct participation of H_2O versus microsolvation. *J. Phys. Chem. A* **112**(41), 10386–10398.
- Nguyen M. T., Raspoet G., Vanquickenborne L. G. and Van Duijnen P. T. (1997) How many water molecules are actively involved in the neutral hydration of carbon dioxide? *J. Phys. Chem. A* **101**(40), 7379–7388.
- O'Leary M. H., Madhavan S. and Paneth P. (1992) Physical and chemical basis of carbon isotope fractionation in plants. *Plant Cell Environ.* **15**, 1099–1104.
- O'Neil J. R., Adami L. H. and Epstein S. (1975) Revised value for the O^{18} fractionation between CO_2 and H_2O at 25 °C. *J. Res. US Geol. Surv.* **3**, 623–624.
- Rudolph W. W., Fischer D. and Irmer G. (2006) Vibrational spectroscopic studies and density functional theory calculations of speciation in the CO_2 –water system. *Appl. Spectrosc.* **60**(2), 130–144.
- Rustad J. R., Nelmes S. L., Jackson V. E. and Dixon D. A. (2008) Quantum-chemical calculations of carbon-isotope fractionation in $\text{CO}_2(\text{g})$, aqueous carbonate species, and carbonate minerals. *J. Phys. Chem. A* **112**, 542–555.
- Stirling A. and Pápai I. (2010) H_2CO_3 forms via HCO_3^- in water. *J. Phys. Chem. B* **114**(50), 16,854–16,859.
- Truhlar D. G. and Garrett B. C. (1984) Variational transition state theory. *Ann. Rev. Phys. Chem.* **35**, 159–189.
- Uchikawa J. and Zeebe R. E. (2012) The effect of carbonic anhydrase on the kinetics and equilibrium of the oxygen isotope exchange in the CO_2 – H_2O system: implications for $\delta^{18}\text{O}$ vital effects in biogenic carbonates. *Geochim. Cosmochim. Acta* **95**, 15–34.
- Uchikawa J. and Zeebe R. E. (2013). No discernible effect of Mg^{2+} ions on the equilibrium oxygen isotope fractionation in the CO_2 – H_2O system. *Chem. Geol.*, in revision.
- Urey H. C. (1947) The thermodynamic properties of isotopic substances. *J. Chem. Soc.*, 562–581.
- Wang B. and Cao Z. (2013) How water molecules modulate the hydration of CO_2 in water solution: insight from the cluster-continuum model calculations. *J. Comput. Chem.* **34**(5), 372–378.
- Wang X., Conway W., Burns R., McCann N. and Maeder M. (2010) Comprehensive study of the hydration and dehydration reactions of carbon dioxide in aqueous solution. *J. Phys. Chem. A* **114**, 1734–1740.
- Wolfsberg M., Van Hook W. A. and Paneth P. (2010) *Isotope Effects in the Chemical, Geological, and Bio Sciences*. Springer, Heidelberg, p. 466.
- Zeebe R. E. (2009) Hydration in solution is critical for stable oxygen isotope fractionation between carbonate ion and water. *Geochim. Cosmochim. Acta* **73**, 5283–5291.
- Zeebe R. E. (2010) A new value for the stable oxygen isotope fractionation between dissolved sulfate ion and water. *Geochim. Cosmochim. Acta* **74**, 818–828.
- Zeebe R. E. and Wolf-Gladrow D. A. (2001) *CO_2 in Seawater: Equilibrium, Kinetics, Isotopes*. Elsevier Oceanography Series, Amsterdam, p. 346.
- Zhang J., Quay P. D. and Wilbur D. O. (1995) Carbon isotope fractionation during gas–water exchange and dissolution of CO_2 . *Geochim. Cosmochim. Acta* **59**, 107–114.

Associate editor: Edwin Schauble